Realizing more accurate OPC models by utilizing SEM contours

Wei, Chih-I, Sejpal, Rajiv, Deng, Yunfei, Kusnadi, Ir, Fenger, Germain, et al.

Chih-I Wei, Rajiv Sejpal, Yunfei Deng, Ir Kusnadi, Germain Fenger, Masahiro Oya, Yosuke Okamoto, Kotaro Maruyama, Yuichiro Yamazaki, Sayantan Das, Sandip Halder, Werner Gillijns, "Realizing more accurate OPC models by utilizing SEM contours," Proc. SPIE 11325, Metrology, Inspection, and Process Control for Microlithography XXXIV, 1132524 (20 March 2020); doi: 10.1117/12.2554527

SPIE.

Event: SPIE Advanced Lithography, 2020, San Jose, California, United States

Realizing more accurate OPC models by utilizing SEM contours

Chih-I Wei*[a], Rajiv Sejpal[a], Yunfei Deng[b], Ir Kusnadi[b], Germain Fenger[b], Masahiro Oya[c], Yosuke Okamoto[c], Kotaro Maruyama[c], Yuichiro Yamazaki[c], Sayantan Das[d], Sandip Halder[d], Werner Gillijns[d]

[a]Mentor Graphics Corporation, Leuven, Belgium;
[b]Mentor Graphics Corporation, Wilsonville, OR, U.S.A.;
[c]TASMIT, Inc., Yokohama-shi, Kanagawa, Japan;
[d]IMEC, Leuven, Belgium

ABSTRACT

The method to perform Optical Proximity Correction (OPC) model calibration with contour-based input data from both small field of view (SFoV) and large field of view (LFoV) e-beam inspection is presented. For advanced OPC models - such as Neural Network Assisted Models (NNAM) [1], pattern sampling is a critical topic, where pattern feature vectors utilized in model training, such as image parameter space (IPS) is critical to ensure accurate model prediction [2-5]. In order to improve the design space coverage, thousands of gauges with unique feature vector combinations might be brought into OPC model calibration to improve pattern coverage. The time and cost in conventional Critical Dimension Scanning Electron Microscope (CD-SEM) metrology to measure this large amount of CD gauges is costly. Hence, an OPC modeling solution with contour-based input has been introduced [6]. Built on this methodology, a single inspection image and SEM contour can include a large amount of information along polygon edges in complex logic circuit layouts. Namely, a better feature vector coverage could be expected [7]. Furthermore, much less metrology time is needed to collect the OPC modeling data comparing to conventional CD measurements. It is also shown that by utilizing large field 2D contours, which are difficult to characterize by CD measurements, in model calibration the model prediction of 2D features is improved. Finally, the model error rms of conventional SFoV modeling and LFoV contour modeling between SEM contours and simulation results are compared.

Keywords: EUV Lithography, SEM Contour, Contour-based OPC Modeling, 5nm, Machine Learning

INTRODUCTION

OPC compact resist model calibration requests adequate IPS coverage and precise wafer data measurements, especially in EUV lithography with critical margin of inter-layers overlay requirement. Conventionally, a cutline-based (gauge) input dataset which includes lithography ADICD information usually requires feature selection and measurements in range of 10,000 gauges to ensure adequate pattern coverage. Due to one-dimensional (1D) nature of gauges, even with such a high number, it is still difficult for a model to predict real two-dimensional (2D) feature shapes based on the cutline-style sampling. As semiconductor technology node keep evolving, feature sizes to next generation nodes is shrinking. In industry N5 and beyond nodes, the higher number of measurement sites are required to maintain design space coverage. Furthermore, stochastic errors such as bridging, pinching and missing features also become significant. It is a challenging task about how to collect and analyze such a huge volume dataset and generate a reliable OPC model.

In figure 1, it shows SEM contour-based OPC modeling solution allows users for reducing metrology tool time and overall model calibration cycle times as well as improving 2D structure predication such as corner rounding, pattern distortion… etc. SEM contour-based modeling comes with its own set of challenges, namely, spiky contour or discontinuities caused by noise, fine center alignment to test structures, contour averaging, a

Metrology, Inspection, and Process Control for Microlithography XXXIV, edited by Ofer Adan, John C. Robinson, Proc. of SPIE Vol. 11325, 1132524 · © 2020 SPIE
CCC code: 0277-786X/20/$21 · doi: 10.1117/12.2554527

robust cost function to account for outliers and the ability to capture high resolution large field of view (LFoV) images for accurate extraction and to capture long range effects.

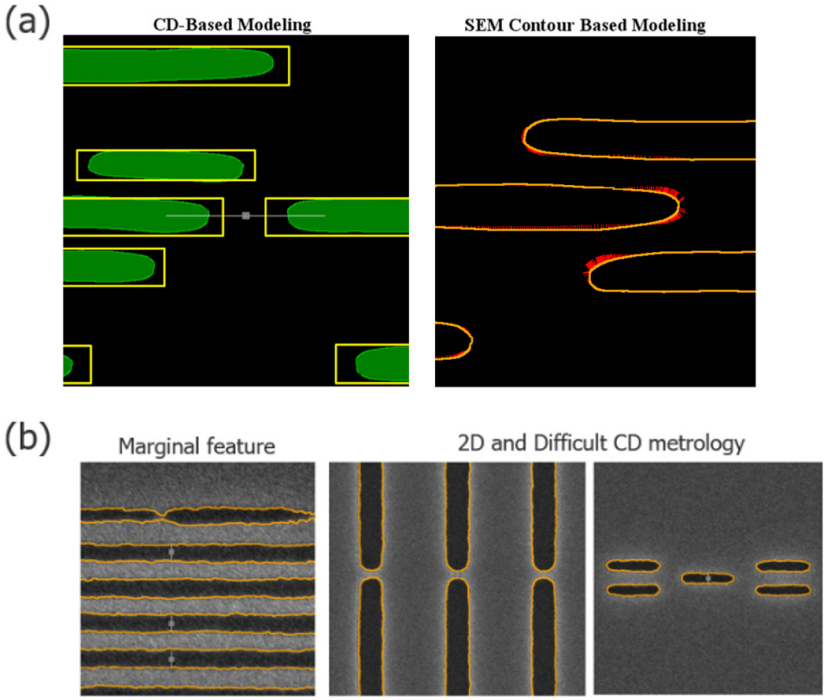

Figure 1, (a) the comparison between cutline-based modeling (left hand) and SEM contour-based modeling (right hand). (b) Shows the clips can be beneficial if we applied contour-based OPC modeling. In gauges-based modeling, it is hard to place right cutline in the center of marginal and difficult 2D regions.

In this paper, we performed OPC modeling among a conventional small field of view (SFoV) contours with cutline-based input and the hybrid-model (both cutline-based gauges and contour-based clips from LFoV) with a contour-based input employing LFoV images (8.0µm * 8.0µm) on 5nm node dimensions. All SEM images are obtained using NGR3500 and SEM contours are extracted by the machine learning algorithm [8]. Figure 2 shows the flow adopted to calibrate contour based OPC models for this experiment. The extracted contours from a top-down SEM images used in conjunction with test features are used as input data along with contour layer information (CLI) file obtained from the metrology tool. CLI is a text file that contains contour description, calculation method, process window conditions for input contours. Moreover, the input data quality checking is quite important for following modeling stages. We will describe the data filtered rules in the third topic of this paper. Within all setups of initial optical model, domain decomposition method mask 3-D model (DDM), input datasets and resist model form accounting for the lithographic processes, the model calibration and results analysis have been done by Calibre® nmModelflow™ and ContourCal™.

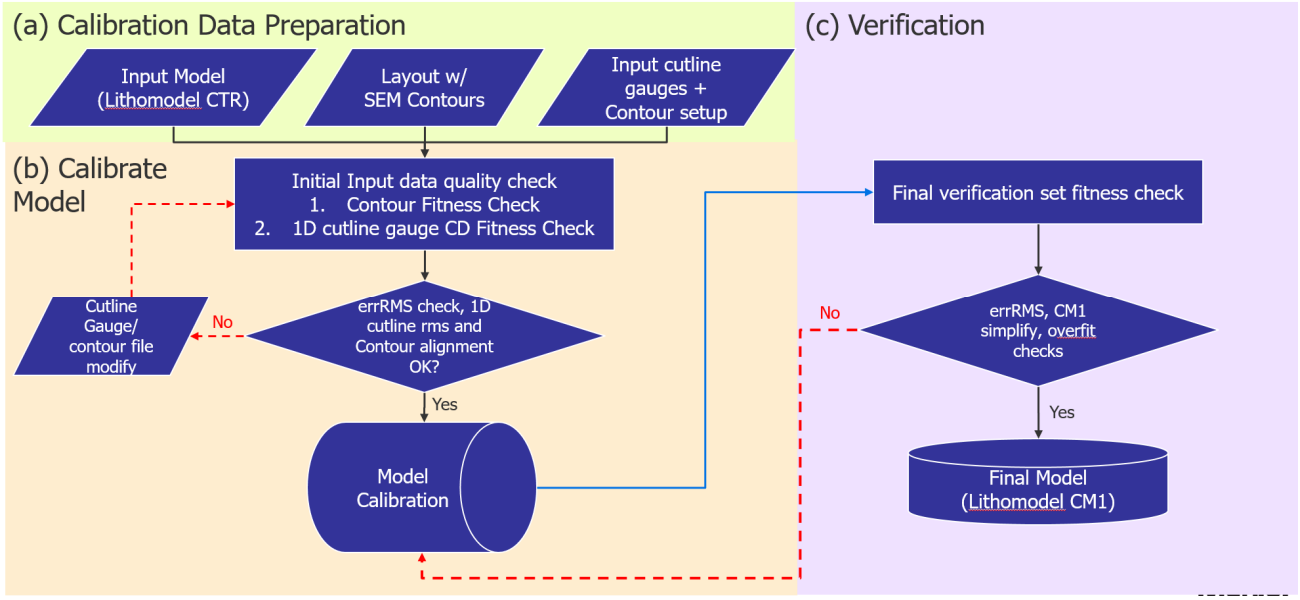

Figure 2, demonstrates the flow chart of (a) the stage 1 in Calibration Data preparation, (b) the stage 2 in model calibration flow and (c) the stage 3 in model validation.

Figure 3 shows brief description of the computational details of Calibre® ContourCal™. RMS_{error} calculated from a set of weighted point-wise error had been used in modeling cost function. Users can also define different area weights in contour clips, and adjust those clips weights for an improved model.

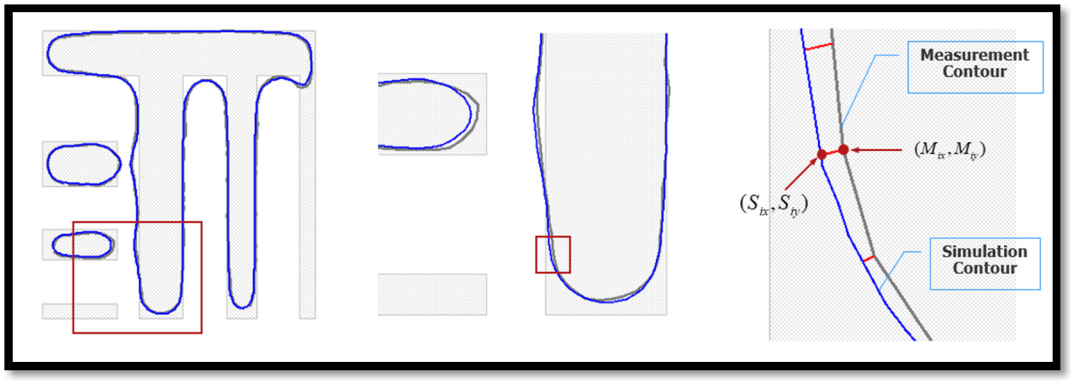

Figure 3, shows cost function or the RMS_{error} used for contour calibration is the measured as the rms of the sum of the weighted point wise error (Di).

$$RMS_{error} = \sqrt{\frac{\sum_{i=1}^{N} w_i {D_i}^2}{\sum_{i=1}^{N} w_i}}$$

And the point-wise error is calculated as:

$$D_i = \sqrt{(S_{ix} - M_{ix})^2 + (S_{iy} - M_{iy})^2}$$

Where S_{ix}, S_{iy}, M_{ix}, M_{iy}, are the normal vectors generated from simulated and measured contours respectively.

Wafer Condition and Metrology tool

1. Wafer and Pattern

Wafer were exposed by ASML's NXE3300 EUV scanner with 13.5nm wavelength and 0.33 NA. Illumination mode is a freeform source in Y-Dipole style and Ta-based mask absorber. The wafer exposure conditions are two-step focus energy matrix (FEM) with a dose step of 3mJ/cm^2 and a focus step of 0.03um. And the lithography process is chemical amplifier resist (CAR) with positive tone developer (PTD) process, which is IMEC baseline process. Feature was completed with anchor CD of 16nm and anchor vertical pitch of 32nm. A variety of test pattern features were selected, consistent with industry node 5nm which includes line-space, tip-to-tip, rectangular holes array …etc.
A standard wafer under layers consisting of substrate, two hard masks and PTD EUV resist is used. A first coarse FEM wafer was used to find the nominal process condition with IMEC data analysis tool ARCADI™. Following with the second retargeting wafer is exposed for 58.6 mJ/cm^2 as nominal dose and -0.11 um as nominal defocus for E/F steps as mentioned above.

2. Metrology tool

In order to achieve large and precise SEM contour, quality of large field SEM image and method to extract precise contour from the SEM image are essential. In this study, NGR3500 Die to Database metrology tool has been applied [6-8]. The tool has a maximum 70μm FoV and a maximum 100MPPS (pixels per second) data rate for imaging patterns on the wafer by SEM. The system has enough data buffer and tens of cluster processors to calculate the huge volume of SEM images in real-time parallelly with image acquisition. While acquiring the SEM images on the wafer, the system clips out target layout data which is stored in GDS-II or OASIS file format on the same area with the SEM image and convert it to the data which can be compared with the SEM image. On the processing system, after aligning the SEM image to the layout data, SEM contour is extracted from each image [9]. By aligning the large SEM image to the layout data, SEM contours are also precise in the layout coordinate system.

3. Performance of large field SEM image

Before acquiring large SEM contour, optimizing image performance with using Key Performance Indicators (KPI) was performed on the metrology system [10]. For KPI, pattern edge sharpness, SNR are evaluated in an image, and repeatability of CD data, stability of image magnification and photoresist shrinkage rate are evaluated in a repeated image acquisitions in the same location of line and space pattern.
However CD measurement repeatability and shrinkage rate has been used as KPI in the traditional 1D CD measurement with small field SEM image, the stability of image magnification and image rotation are also critical KPI in the large field SEM contour, because the larger image is applied, the more critical geometry distortion effect is at the peripheral of the image. These KPI had been evaluated with different landing energy by continuous image acquisition at same location.
As a result of the optimization, condition with 1500eV of landing energy and 8.0μm * 8.0 μm FoV was chosen for this study by considering the image stability. With this condition, CD measurement repeatability (3σ) on the line pattern of 100nm length and photoresist shrinkage rate are 0.17nm and 1.7nm respectively as shown in Figure 4 (a). The stability (3σ) of the image magnification and the image rotation are 0.009% and 0.006 degrees respectively as shown in Figure 4 (b). In terms of throughput, 138 large SEM images can be acquired in an hour with this condition.

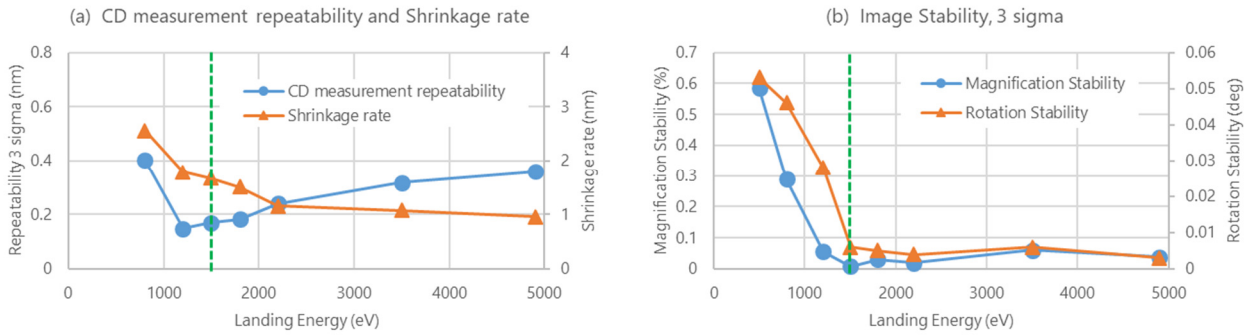

Figure 4, (a) CD measurement repeatability and Shrinkage rate. (b) Stability of large field SEM image in magnification and rotation

4. Contour extraction

Optimal condition was applied to target wafer and the pattern contour could be extracted from large field SEM image as shown in Figure 5. Die to Database and machine learning algorithm were applied for extracting large field SEM contour. The model of machine learning could be trained on the target wafer and it finish in 60 seconds. And contour extraction with calibrated model is also faster than image acquisition and it will not be bottleneck of throughput of image acquisition.

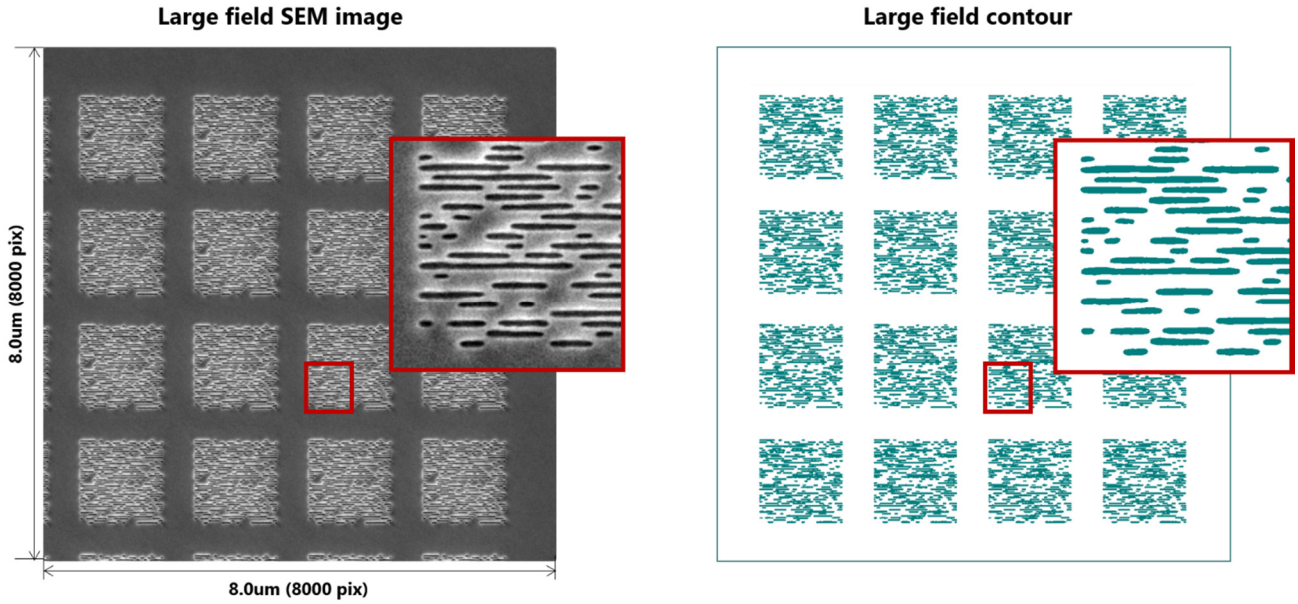

Figure 5. 8μm large field SEM image and extracted contour

Result and discussion

1. Test plans on SFoV and LFoV

We planned to test the model converge and precision by utilizing both SFoV and LFoV contours which extracted by NGR. In the SFoV experiment, total 1061 nominal and 602 PWCs gauges were selected for model calibration and verification. The test pattern for the conventional SFoV OPC modeling are included LS/Multi-LS/2-Bars/T2T/short slots pattern types. Meanwhile, line and space ADICD had filtered by the consideration of fine process window. When ADICDs in 1D lines are larger than 15nm, space are larger than 16nm, 2D slot-type widths are larger than 17nm, and line-end tip to tip spaces are larger than 14nm would be take into modeling. Furthermore, only 50% of nominal gauges were brought into model calibration, and total gauges were formed a verification set. After the cutline-based gauge file was ready, the model calibration applied with nmModelflow™ with various Compact Model 1 (CM1) model forms.

In the LFoV experiment, the pre-processing of the contours isnecessary before we puts those contour clips into modeling. Firstly, the 16 separated repetitive contours were overlapped precisely onto one location with its post-OPC (see figure 7). Afterward, we classified the contours according to their quality (please see the details in section 3 of this topic). Moreover, Calibre® ContourCal™ provides fine contour average and alignment functionalities which help removing high frequency spiky shapes and setting better contour locations. It usually improves the precision of the input contours by a remarkable amount. In the contour-based model calibration, we also compared the model precision between cutline-based inputs which manually drawing on LFoV contours and the filtered contour-based inputs. By analyzed the IPS and simulation contours, the quality of the models could be demonstrated.

2. SFoV CD average and modeling results

The conventional cutline-based OPC modeling shows good converge results by SFoV SEM input CD data. Typically, the SEM FoV is between 0.512μm * 0.512μm to 1.0μm * 1.0μm. In this section, we firstly check the SFoV contours whether they are adequategood enough to generate a converged OPC model by conventional approach. Here, we used SFoV contours of 1061 nominal and 602 PWCs for the optical model optimization and the resist model calibration. Although the edges of the contours is quite smooth, the CD averaging of 1D array and identical 2D area should be performed before input into modeling.

In figure 6, it shows the results used Calibre® OPCVerify™ tool to extract the average CD from SFoV contours by various sizes of measurement box. From 20nm to 1200nm length of measurement box, it could be observed that contour CD fluctuation caused by noise/litho process can be reduced remarkably. The saturated CD_diff error rms is less than 0.05nm if we apply box size larger than 300nm, which we applied in all 1D CD gauges. In 2D gauges, there is no way to perform similar modification on CD. Therefore, only the cutline CDs with identical environments would be averaged.

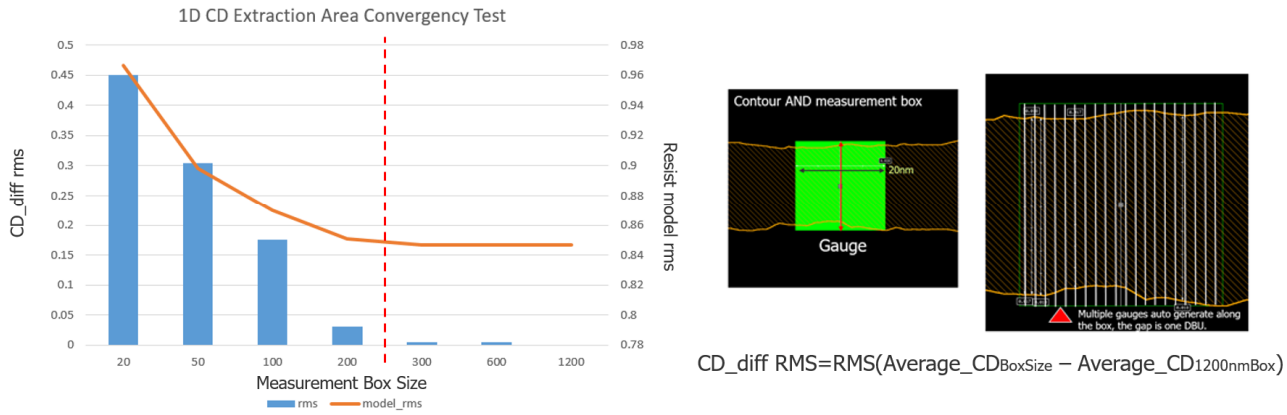

Figure 6, right hand two figures shows the methodology of CD averaging. We applied rms calculation on all 1D gauges among various averaging measurement box length (from 20nm to 1200nm). In left hand side, it shows the CD_diff rms vs measurement box size and simple CM1 model rms vs measurement box size.

After the 1D and 2D gauges are processed for modeling, a random gauge selection by optical signature had applied with nmModelflow™ "optical similarity gauge split" functionality [11]. 50%-50% gauges were split into calibration gauges and verification gauge sets. Then, EUV optical model with wafer process filmstack and DDM model with correct mask film stack were prepared for resist modeling. A 87 degrees sidewall slope of the mask absorber and 1nm (1x) mask bias with 10nm corner chop were also applied to improve the 2D model accuracy. Also, PWCs gauges were only used for selecting best beam focus (BF)/ defocus start (DS) combination based on Bossung matching of best focus.

	SFoV Model Calibration and Verification			
	Calibration Set		Verification Set	
Model Form Splits	1D cutline rms	2D cutline rms	1D cutline rms	2D cutline rms
Job1 (CTR)			1.931	2.692
Job2 (MF22)	1.221	1.506	1.334	1.473
Job3 (MF22 + Curvature)	0.809	1.052	0.846	1.064
Job4 (MF22 + Multi-Range SEM Shrinkage)	1.102	1.366	1.163	1.281
Job5 (MF22 + Multi-Range SEM Shrinkage + Curvature)	0.71	0.979	0.755	0.974

Table 1, the modeling job slips and corresponding calibration/ verification sets error rms in SFoV.

Various CM1 model forms were tried, Table 1 summarizes and compares the most promising results with the optical only and CM1 model form 22 and various resist kernels. Among those 5 jobs, 1. Job1 was using constant threshold resist model (CTR), 2. Job2 was using MF22 (2 diffused acid, 1 base, 1 slope, I_{max}, I_{min} and 1 laplacian terms), 3. Job3 was using MF22 plus curvature term, 4. Job4 was using MF22 plus multi-Range SEM shrinkage term, 5. Job5 was using MF22 plus multi-Range SEM shrinkage and curvature terms.

The Job5 shows model form 22, SEM shrinkage and Curvature Terms can get the best overall 1D and 2D model error rms. The average error rms can reach less than 1nm. Furthermore, 1D error range is +/- 2.3nm, and 2D is +/- 3nm.

Comparing the 2D verification sets of Job2/Job3 and Job4/5, model precision could benefit remarkably among 24% to 28% improvement with Curvature Term of CM1. Moreover, 1D gauges also benefit from the curvature term significantly, among 35% to 36% precision improvement can be observed. The reason might be curvature term help the converge on 2D part without heavy threshold adjustment, therefore the 1D can achieve better error rms due to the preferable threshold. In general, SFoV OPC modeling practices with NGR contours shows great potential to generate quality OPC model with conventional cutline-based input.

3. LFoV contour utilization and modeling results

In LFoV contour-based modeling, total 30 large clips were used for model calibration/ verification. However, not all the contours could be used for modeling due to the proper requirement of images/contours quality. The quality of images and contours depend not only on the stability of metrology but also on a fine lithography process. Therefore, the input contours for OPC modeling should be selected carefully. In this paper, we introduce the methodology to investigate the image and process quality by contour's variation band (VB).

In Figure 7, it shows the approach of how to classify the input contours. There are two metrics of long edge (Edge VB) and line-end edge (Line-end VB) taken into account due to pattern symmetricity. Since the SMO source is Dipole-Y-like. The VBs in long edges would be less than that in line-end edges due to the image contrast would be higher on the horizontal edged than that of vertical.

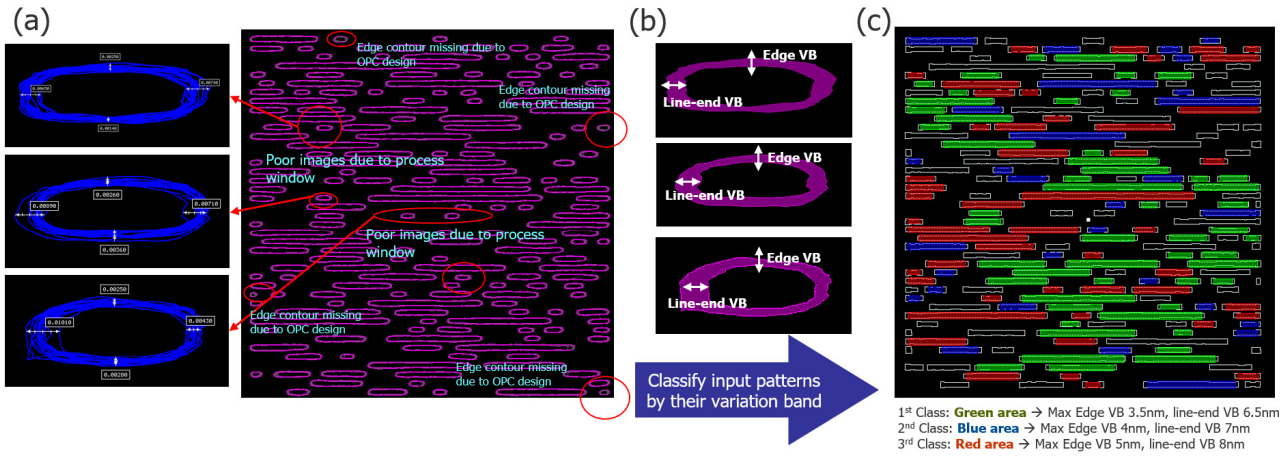

Figure 7, (a) shows the overlapped nominal contours in one LFoV clip. (b) Shows the variation band (VB) which is most outer overlapped contours subtract most inner overlapped contours. (c) Shows the classified area among different criteria which we used in this paper.

In step (a) of figure 7, firstly the contours of all 16 repeated small clip in the same LFoV were overlapped with proper shift amounts. From the left-hand figure of (a), multiple-contours demonstrated the variation of the process/ metrology noise. The VB in (b) was created by subtracting the most outer contours with the most inner contours. Finally, according to the specific Edge VB and Line-end VB conditions, locations with large VB conditions were filtered out and locations selected for contour-based model calibration or verification.

In Figure 8, it shows the band width analysis of both Edge VB and Line-end VB. This is a histogram of the Edge VB and Line-end VB, which demonstrated the VB vs Edge counts of the total identical polygons in LFoV images.

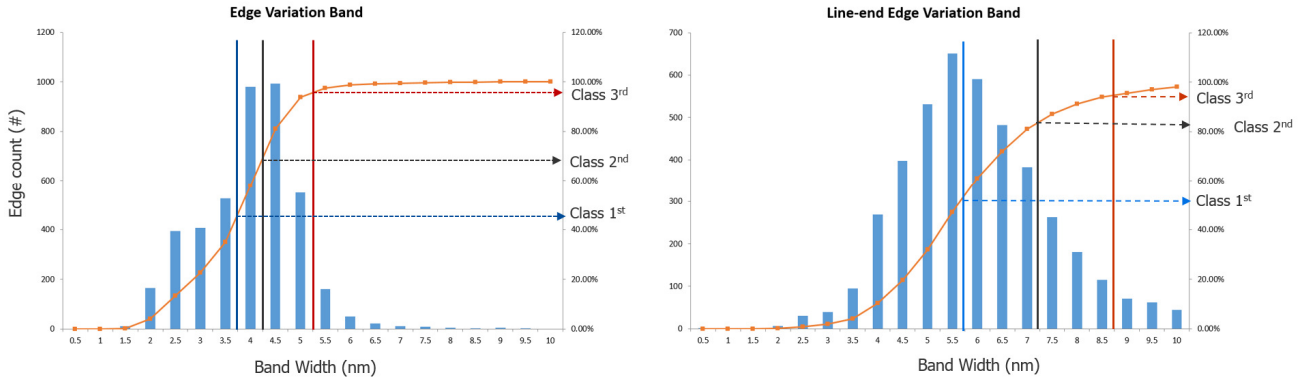

Figure 8, left hand chart shows the band width vs edge counts in Edge VB, and right hand chart shows the band width vs edge counts in Line-end Edge VB. The orange curve shows the cumulative percentage of the polygon edges. And the blue/black/red split lines are used to classify the band width to the specific categories.

The non-Gaussian distribution of the VB exhibited the contour variation through possible causes. It includes the process variation, the image sampling noise, and pattern center shifting. We firstly pick up the ~50% of the total edge counts as first class in both VB metrics. Then, 2nd class criteria is slightly different from Edge VB and Line-end VB for among 70% ~80% of total edge counts. In the last 3rd class, it covered almost all edge counts (more than 95%). Out of 1911 unique contours, total 126 contours are classified into Class 1st, 214 contours are Class 2nd, 533 contours are Class 3rd. The rest of the contours will not be used in the following contour-based modeling and verification.

After the contours are filtered and classified, Calibre® ContourCal™ provides fine contour averaging and alignment functionalities which help removing high frequency shapes and setting better contour locations. In this test case, after averaging and alignment, the contours to optical model simulation EPE of Class 1st can be further reduced from 13nm to 9nm. (30% precision improvement)

	LFoV input				
	Calibration Set		Verification Set		
MF28 + curvature	Cutline rms (CD based)	Contour Clip rms (EPE based)	Cutline rms (CD based)	Contour Clip rms (EPE based)	Contour Clip error range
Job1 (Cutline input)	1.166		1.129	1.18 (filtered)	12.01 (filtered)
Job2 (Calibration set with Class 1)		0.978	1.53	0.978	9.31
Job3 (Calibration set with Class 1+2)		0.94	1.52	0.925	7.92
Job4 (Calibration set with Class 1+2+3)		0.96	1.57	0.969	8.45

Table 2, the modeling job slips and corresponding calibration/ verification sets error rms in LFoV.

In LFoV model calibration, we setup 4 different jobs which used different combination of input cutline/contours for model convergence tests. In Table 2, the first job is cutline-based input dataset. The orthogonal cross cutlines anchored at the center of each LFoV contours have been placed manually according to all classes. Total 302 cutline-based gauges out of total 602 gauges for calibration set, and overall gauges formed a verification set Calibration gauges set was also picked by nmModelfow™ "optical similarity gauge split" functionality.

The rest of the three jobs from the upper table are correlated to contour-based input data set. In Job2, the class 1st was used for model calibration. In Job3, it was calibrated with class 1st and 2nd, where we applied lighter weight on 2nd contour input data. In Job4, we combined Job3 input along with 50% class 3rd contours as input data, and treated them with different calibration weights. After the jobs finished, all candidate OPC models were brought into verification datasets which contain the cutline-based 602 gauges and all classes of the

contours. Comparing Job1 to Job 2/3/4, it shows contour clip error rms is lower than 1.2 though, however, several simulation clips could not be resolved, which goes against to the wafer data.

It can also be observed that the Job2 and Job4 got very similar results in both calibration and verification error. Moreover, Job3 had the best performance over Job4, which indicates the importance of modeling input dataset quality. The contour clip average error rms is less than 1nm (EPE based) and the error range is +/- 4nm in LFoV random logic area.

The IPS was also analyzed for the various classes of data, as seen in Figure 9.

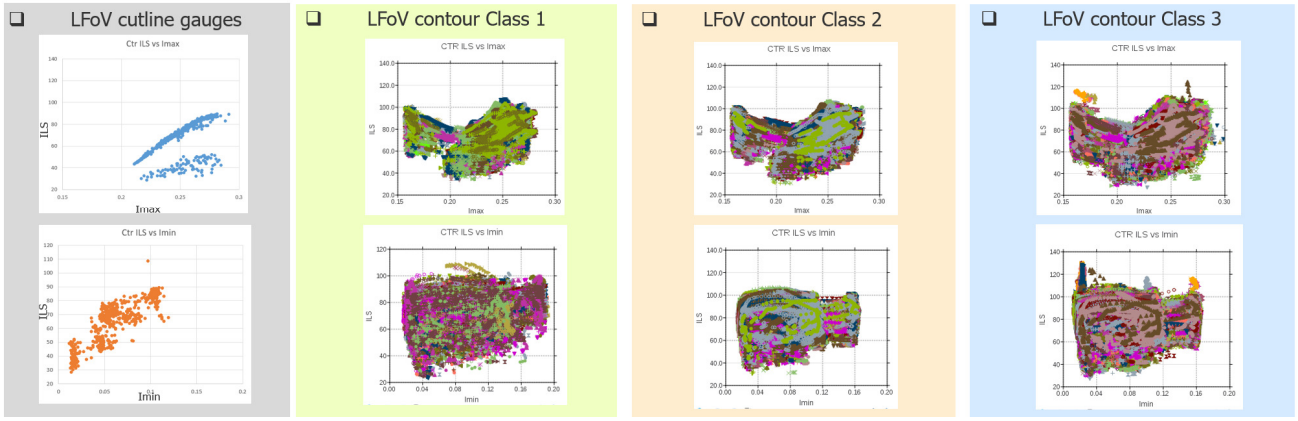

Figure 9, it shows the ILS vs Imax/Imin IPS plots from the most left hand side, LFoV cutline-based gauges to most right hand side contour class 3rd.

Considering the (ILS vs I_{max}/I_{min}) IPS coverage plots, obviously cutline gauges used in Job1 had very poor IPS coverage, which can explain why some patterns had poor performance in verification set, since those pattern were not covered well in IPS. Consequently, the features which are far away from the coverage area may have poor prediction.

From Class 1st to Class 3rd, it was confirmed almost Class 3rd area could be covered by previous Class 1st and 2nd. It means that the inclusion of class 3rd into the model calibration did not show meaningful improvement in the verification results, it should have less impact on the model coverage but degraded results by introducing more noise in modeling input data. It might explain why Job4 gets poor results than Job3.

In Figure 10, it shows the details of Job1 vs Job3 contour clips verification results.

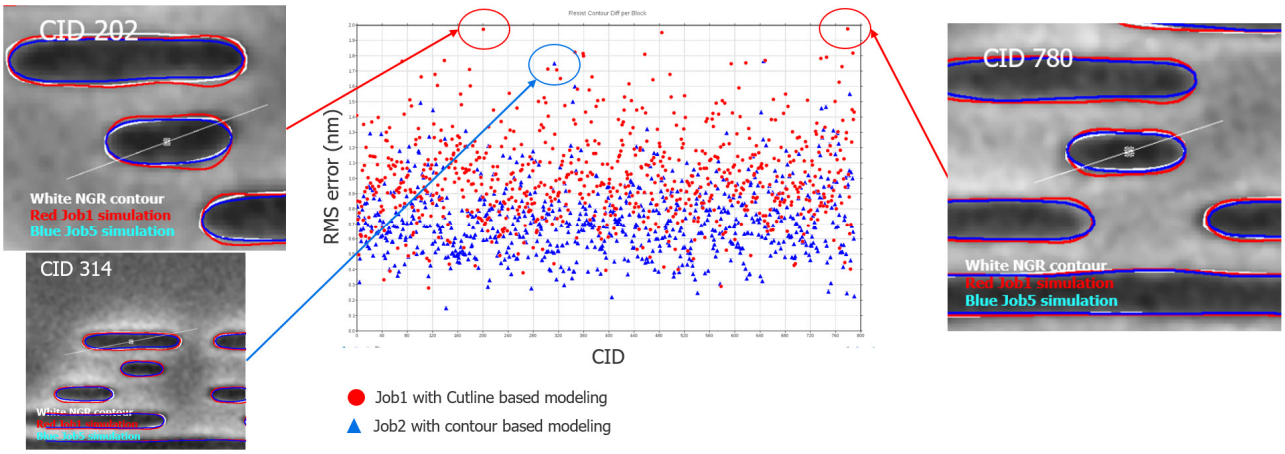

Figure 10, the center plot shows the overlapped error rms distribution of job 1 and 2 from all Clip ID (CID). The top-down SEM images on the two sides, the white one is extracted contours from SEM images, the red one job1 contours and blue one is job2 contours.

If the error rms results are examined closely, the distribution of all clips ID (CID) between Job1 and Job2, only CID-314 of Job2 has poor error rms over that of Job1. Otherwise, Job2 has better error rms on 2D contour verification in each CID. In CID-202, it is obvious that the red simulated contours from Job1 match NGR measured contours in the tip or flat edge, but they are distorted in the corners part of the 2D slots, especially the slot length is short.

As a result, modeling approach includes contour-based input data would be a benefit for a better 2D fitness as our expectation.

SUMMARY

Calibre® ContourCal™ modeling toolkit with NGR3500 metrology demonstrated both good results on conventional SFoV (0.5µm * 0.5µm) OPC modeling and LFoV (8.0µm * 8.0µm) contour modeling capability on 5nm node EUV wafer. In both cases, the 1D and 2D RMS_{error} can be less than 1nm, which demonstrated a great potential of good OPC modeling by utilizing SEM contour clips.

In LFoV modeling experiments, contour clips generated much larger IPS coverage than conventional cutline-based gauges methodology, because the complicated environment of random logic contain massive information in a single polygon. Hence, the contour-based modeling shows better results in verification dataset.

Measured SEM contours enable variation band analysis of each individual pattern. By careful filtering the input data, 3 classes of contour sets were defined. Model calibration experiments shows better model accuracy and prediction by utilizing the first two classes instead of all data available. Therefore, good input contours data quality (lower VB but larger IPS coverage) could generate better OPC model than that of lump sum input data. Furthermore, LFoV metrology and contour modeling shows great potential in future EPE modeling with AEICD data/contour, Hotspot modeling and CD Distribution/LER/LWR/Stochastic modeling.

Acknowledgement

The authors wish to thank Andrew Burbine for the discussion of IPS coverage, Edita Tejnil for the discussion of feature selection. Stewart Wu for the task support during this study. Thanks to all the Mentor Graphics and

TASMIT co-workers who involved to this project. We also want to thank Jeroen Van de Kerkhove (IMEC) for great development of ARCADI which supported the initial anchor CD inspection of the experiment wafer.

This project has received funding from the ECSEL Joint Undertaking (JU) under grant agreement No 783247. The JU receives support from the European Union's Horizon 2020 research and innovation program and Netherlands, Belgium, Germany, France, Austria, United Kingdom, Israel, Switzerland.

REFERENCES

[1] Kostas A., Shashidhara G., Clement M., Kostya S., Michael L., Andrew B., Germain F., Yuri G., *"Using machine learning in the physical modeling of lithographic processes,"* in Proc. SPIE 10962, Design-Process-Technology Co-optimization for Manufacturability XIII, 109620F (4 April 2019)

[2] Ralph E. Schlief, *"Effect of data selection and noise on goodness of OPC model fit,"* in Proc. SPIE 5754, Optical Microlithography XVIII, (12 May 2005)

[3] Yuyang S., Yee M. F., Yingfang W., Jacky C., Dongqing Z., Shaowen G., Nanshu C., Byoung Il C., Antoine J. B., Mu F., Jianhong Q., Stefan H., Liang L., Wenjin S., *"Optimizing OPC data sampling based on "orthogonal vector space","* in Proc. SPIE 7973, Optical Microlithography XXIV, 79732K (22 March 2011)

[4] Georg V., Brian W., Hans-Juergen S., *"Pattern selection in high dimensional parameter spaces,"* in Proc. SPIE 8326, Optical Microlithography XXV, 832618 (13 March 2012)

[5] Jim V., Ovadya M., Dan L., Ofer L., Youval N., George E. B., John S., *"SEM-contour based OPC model calibration through the process window,"* in Proc. SPIE 6518, Metrology, Inspection, and Process Control for Microlithography XXI, 65180D

[6] Kitamura, T. et al., *"Introduction of a Die-to-Database Verification Tool for the Entire Printed Geometry of a Die: Geometry Verification System NGR2100 for DFM,"* Proc. SPIE 5756(2005).

[7] Sayantan D., Ryo S., Shinji M., Sandip H., Kotaro M., Philippe L., Yuichiro Y., *"E-beam inspection of single exposure EUV direct print of M2 layer of N10 node test vehicle,"* in Proc. SPIE 10959, Metrology, Inspection, and Process Control for Microlithography XXXIII, 109590H (26 March 2019)

[8] Sato, Y. et al., *"Edge placement error measurement in lithography process with die to database algorithm,"* Proc. SPIE 10959(2019).

[9] Yosuke O., Shinichi N., Akinori K., Tsugihiko H., Taihei M., Kotaro M., Seulki K., Yuichiro Y., *"Contour extraction algorithm for edge placement error measurement using machine learning,"* in Proc. SPIE 11325, Metrology, Inspection, and Process Control for Microlithography XXXIV

[10] Chia-Jen L., Chia-Hao T., Po-Chung C., Yoshishige S., Shang-Chieh H., Chu-En., Kotaro M., Yuichiro Y., *"Quantitative Approach for Optimizing e-beam Condition of Photoresist Inspection and Measurement,"* in Proc. SPIE 10585, Metrology, Inspection, and Process Control for Microlithography XXXII, 105852W (13 March 2018)

[11] Edita Tejnil, *"Application of optical similarity in OPC model calibration,"* in Proc. SPIE 10147, Optical Microlithography XXX